Research Square

Preprints are preliminary reports that have not undergone peer review.
They should not be considered conclusive, used to inform clinical practice,
or referenced by the media as validated information.

M1 Macrophage Derived Exosomes As Platform For CD47 Immune Checkpoint Blockade And Chemotherapy Delivery

Xin Bao
Second Affiliated Hospital of Soochow University
Feng Yuhan Feng
Suzhou Institute of Nano-tech and Nano-bionics
Chen Dong
Ningbo University of Finance & Economics
Mingsheng Xu
Suzhou Institute of Nano-tech and Nano-bionics
Guoqin Jiang
jiang_guoqin@163.com

Second Affiliated Hospital of Soochow University

Article

Keywords: Exosomes, M1 macrophages, CD47, SIRP-α, Doxorubicin, Cancer immunotherapy

Posted Date: July 31st, 2026

DOI: https://doi.org/10.21203/rs.3.rs-10301984/v1

License: This work is licensed under a Creative Commons Attribution 4.0 International License.
Read Full License

Additional Declarations: No competing interests reported.

Abstract

Cluster of Differentiation 47 (CD47) counteracts immune activity upon binding with Signal-Regulatory Protein alpha (SIRP-α) in various malignancies. Exosomes derived from M1 Macrophage (M1-Exo) represent a potential immunotherapeutic strategy to combat malignancy through tumor cell interaction. Here, the inheritance of SIRP-α on M1-Exo was revealed, and Doxorubicin loaded M1-Exo was constructed to antagonize CD47 and enhance chemotherapy delivery. Western blotting confirmed the presence of SIRP-α on M1-Exo, which interacts with cancer cells through binding and endocytosis. Delivered Doxorubicin further potentiates cancer apoptosis. The delivered doxorubicin further potentiates cancer cell apoptosis. These exhibited properties of M1-Exo set the stage for future re-engineering to reinforce targeting and delivery platforms.

1. Introduction

Extracellular vesicles (EVs) are heterogeneous liposomes that facilitate the transport of intercellular cargo and intercellular signals, and reflect cell status. EVs are categorized based on size and origin, as well as by surface marker proteins that suggest their functions. However, due to their high heterogeneity, these classifications remain largely uncertain and require further investigation [1]. Based on size, EVs are divided into exosomes (30–200 nm), microvesicles (MVs) (200–1000 nm), ectosomes (often synonymous with MVs), and apoptotic bodies (ABs) (1–5 μm). Exomeres (< 30 nm) and oncosomes (1–10 μm) were identified in 2018, but their functional overlaps with other EVs remains unknown [1]. Exosomes, due to its high biocompatibility, immunogenicity, flexibility, and innate targeting and transporting functions is a promising tool for drug delivery [2]. The formation and secretion of exosomes, in contrast to ectosomes (which bud outward from the cell membrane), occur through inward budding to form early sorting endosomes (ESE) via clathrin-mediated endocytosis (CME), clathrin-independent endocytosis (CIE), and clathrin-caveolin-independent endocytosis. These processes all depend on signaling related to the final functional goal of the exosome [3]. Proteins such as CD63, which belongs to the tetraspanin superfamily, are thus incorporated into exosomes and serve as important markers [4].

Immune checkpoint inhibitors (ICI) function by targeting specific, overexpressed markers on cancer cells that facilitate immune evasion. Inhibition of such checkpoints recruits immune cells that ultimately induce cancer destruction [5]. Traditionally, ICI inhibition is approached through the chemical synthesis of monoclonal and bispecific antibodies (mAbs and biAbs), acting as antagonists for single or dual immune checkpoints, such as PD-1 via Nivolumab, and Cemiplimab. However, issues with traditional ICIs include lack of specificity due to tumor heterogeneity, poor tumor penetration, and the risk of immune-related adverse events (irAEs) [6]. Utilizing immune cell-derived ICI protein along with smart nanocarriers is an effective and comparatively non-intrusive approach, addressing the issues of traditional ICIs. Followed by recent developments in smart nanocarriers, such as photodynamic Exosomes [7], Immune cell derived nanocarriers thus is a novel and diversely compatible system for Immunotherapy.

Macrophages are phagocytic immune cells classified in the mononuclear phagocyte system (MPS). During the embryonic stage, tissue-resident macrophages differentiate from hematopoietic stem cells (HSCs), bone marrow-derived progenitors, or local embryonic precursors [8]. They are one of the primary immune cells that differentiate from local stem cells during embryonic stage [9], whereas monocyte derived macrophage first circulates in the blood and then implant themselves into tissues after cytokine, PAMPs/DAMPs, or environmental cues [8]. Classically activated macrophage and alternatively activated macrophage are respectively called M1 and M2 Macrophages. M1 macrophages are induced by LPS, IFN-γ, TNF-α, etc.; they possess pro-inflammatory characteristics and are mainly characterized by CD86, TNF-α, MHC-II, and SOCS3. It secretes proinflammatory cytokines such as interleukin-1β (IL-1β), IL-6, and TNF-α. M2 Macrophage performs anti-inflammatory and tissue repair tasks; It is induced by IL-4, IL-13, and TGF-β, and is furthermore characterized into M2a, M2b, M2c, and M2d (TAMs) under different circumstances [1]. Macrophages are highly plastic; they dynamically alter their phenotypes based on the local microenvironment [10]. This versatility exists as a continuum between the M1 and M2 states, driven by metabolic reprogramming and Epigenic regulations [11–12]. This property is vital for tissue homeostasis, inflammation/anti-inflammation, etc. Pathologically, maladaptive macrophage phenotypes display direct or auxiliary support to pathogenesis, such as carcinogenesis, tissue fibrosis, and autoinflammatory diseases [13].

The SIRP-α/CD47 axis, or the “do not eat me” signal is a critical ICI in Immunotherapy. Structurally, CD47 is a five transmembrane domain protein with an extracellular IgV domain; SIRP-α is a receptor with three Ig-like extracellular domains. This signal was first found on circulating HSCs and red blood cells to evade phagocytosis [14]. Cancer cells utilize the same mechanism. Thus, blockade of SIRP-α/CD47 axis by ICI is significant. Additionally, an increase in Cancer endocytosis and Macrophage antibody dependent cellular phagocytosis (ADCP) is observed [15–16].

In this study, we therefore propose and investigate a novel bifunctional platform utilizing M1 Macrophage-derived Exosomes (M1-Exo) for the delivery of a CD47 immune checkpoint inhibitors and a chemotherapeutic agent (e.g., Doxorubicin). We hypothesize that this M1-Exo system can: (i) achieve immune checkpoint blockade specifically and stably; and (ii) synergize with the delivered chemotherapy to directly kill cancer cells and enhance anti-tumor immune responses. By integrating these therapeutic mechanisms, this study aims to establish a safe and effective nanoplatform that overcomes the limitations of conventional ICI therapeutics and advances the field of cancer immunotherapy (Fig. 1).

Figure 1. Schematic illustration of the formation of M1-Exo from M1 Raw 264.7 cells, electroporation-mediated drug loading of M1-Exo, and the interaction of M1-Exo/DOX with B16F10 cells.

2. Materials and Methods

2.1 Cell culture

Raw 264.7 cells were cultured in Dulbecco's modified Eagle's medium (DMEM) supplemented with 15% fetal bovine serum (FBS) and 0.83 U/mL lipopolysaccharide (LPS). B16F10 cells were cultured in DMEM supplemented with 15% FBS. The cells were incubated at 37°C with 5% CO_2. Both cell lines were obtained from the Cell Bank of the Chinese Academy of Sciences (Shanghai, China). DMEM and FBS were ordered from Gibco.

2.2 Cells immunofluorescent assay

Raw 264.7 cells were gently washed with phosphate-buffered saline (PBS) two to three times and then fixed with 4% paraformaldehyde. Then the cells were permeabilized using 3% BSA containing 0.05% Triton X-100. After that, the cells were incubated with antibodies against CD16 and SIRP-α for 4 h at room temperature (RT). After being washed with PBS for 15 min, the cells were then incubated with Alexa Fluor 647-conjugated anti-rabbit secondary antibodies for 2 h at RT. Finally, the cells were observed using super-resolution microscopy (Nikon).

2.3 Isolation of M1-Exo from Raw 264.7 cells

Exosome Isolation protocol refers to previously well-established methods [26, 27]. M1-Exo is isolated from cell culture medium. The cells are cultured through previous steps and transferred into Exosome free medium and cultured for 72 h. Afterwards, the cell culture medium was collected and first centrifuged at 800g for 10 min and then at 2,000g for 10 min. The pellets were discarded. Then, the supernatant is centrifuged at 10000g for 30 min to remove Microvesicles. Finally, the supernatant is centrifuged at 100000g for 90 min to pellet Exosomes. All the centrifugation is done at 4°C. Exosomes were suspended in exosome freezing medium and stored at -20°C for short-term storage or at -80°C for long-term storage.

2.4 Characterization of Exosomes

M1-Exo were diluted 1:100 in phosphate-buffered saline (PBS), and the size was measured via nanoparticle tracking analysis (NTA). The Zeta Potential of M1-Exo was analyzed by electrophoretic light scattering (ELS). The morphology of M1-Exo was examined by transmission electron microscope (TEM). M1-Exo were added onto a glow-discharged carbon-coated grid for 15 min and then covered with 3% uranyl acetate stain.

2.5 Exosome Drug loading

Exosomes were loaded with doxorubicin using a Bio-Rad electroporator at 300 V, with a final doxorubicin concentration of 0.15 μg/mL. The loading concentration was determined by lysing M1-Exo/DOX with RIPA buffer and comparing the autofluorescence to an established standard curve. The loaded exosomes were then separated from free doxorubicin using a 100 nm pore size centrifugal filter (Millipore) at 1,500g for 15 min, twice.

2.6 Western Blot

The Cell and Exosome are lysed using RIPA buffer (Beyotime). Then the protein was heated at 100°C for 10 min for complete denaturation and separated on 15% or 10% SDS-PAGE gels at 60–90 V. Then, the proteins were transferred to the polyvinylidene fluoride (PVDF) membranes. Then the protein was transferred at 80 V for 2.5 hours with constant cooling. The transferred membrane was blocked with 5% milk at room temperature (RT) for 1 hour. Primary antibodies against SIRP-α (Abcam, ab53721), CD16 (Abcam, ab203883), PD-1 (Abcam, ab214421), CD63 (Abcam, ab217345), caspase 3 (Abcam, ab2787), Na^+/K^+-ATPase (Abcam, ab76020), and β-actin (Santa Cruz, 2Q1055) were applied to the membranes overnight at 4°C. HRP-conjugated secondary antibodies were applied to membranes for 1 h at RT. Finally, chemiluminescence was detected using a Tanon image analysis system with enhanced chemiluminescence substrate (Thermo Fisher Scientific) .

2.7 In vitro binding assay

M1-Exo were previous labeled with Alexa Flour 647. Then M1-Exo (100 μg/mL) were incubated with B16F10 cells, which had been seeded in confocal imaging dishes, at 37°C for 15 min. Afterwards, the cells were observed by confocal microscope (Nikon).

2.8 In vitro cytotoxicity of M1-Exo and M1-ExoDOX

The cytotoxic effect of M1-Exo on tumor cells was evaluated using the Cell Counting Kit-8 (CCK-8) assay (Beyotime, C0038). B16F10 cells were seeded into 96-well plates at a density of 1×10^4 cells per well and allowed to adhere overnight. The cells were then treated with varying concentrations of M1-Exo (5, 10, 20, and 40 μg/mL) for 24 h at 37°C. Subsequently, the culture medium was replaced with fresh medium containing 10% CCK-8 solution, and the plates were incubated for an additional 2 h at 37°C. Absorbance was measured at 450 nm using a microplate reader (e.g., Thermo Scientific Varioskan LUX or equivalent). Cell viability was calculated as the percentage relative to untreated control cells.

Apoptosis induced by DOX-loaded M1-Exo (M1-ExoDOX) was assessed using the APC Annexin V Apoptosis Detection Kit with PI (BioLegend, 640932). B16F10 cells were cultured in 12-well plates until reaching approximately 80% confluence and then treated with M1-ExoDOX (100 μg/mL) for 24 h at 37°C. After treatment, cells were harvested, washed, and stained with Annexin V-APC and PI according to the manufacturer's instructions. Stained cells were immediately analyzed by flow cytometry using a Beckman Coulter CytoFLEX system. Data were processed using CytExpert software (Beckman Coulter).

2.9 Statistical analysis

All data presented represent the results from multiple independent experiments and are shown as mean ± SD unless otherwise stated. GraphPad Prism (GraphPad Software) was used for all calculations. Data comparisons were performed with one-way analysis of variance (ANOVA). A difference of $p < 0.05$ was considered statistically significant; ns: not significant ($p > 0.05$).

3. Results

3.1 The polarization and characterization of M1 Macrophage

To derive M1-Exo that inheritably expressed SIRP-α and exhibited inflammatory characteristics, M1 macrophages were successfully derived from M0 macrophages. Lipopolysaccharide (LPS) was incubated with M0 Raw 264.7 cells for 24 h prior to exosome isolation. A morphological change from the “disk-like” M0 Raw 264.7 cells to slightly elongated M1 Raw 264.7 cells was initially observed (Fig. 2a). Then, the optimal LPS concentration for polarizing M1 Raw 264.7 cells was determined via flow cytometry analysis of M1 macrophage markers CD80 and CD86 (Fig. 2b). Furthermore, super-resolution imaging revealed membrane expression of CD16 and SIRP-α on pseudopods of M1 Raw 264.7 cells. Clear nanoclusters of CD16 and SIRP-α on pseudopods, which are high-frequency sites of endocytosis, suggest inward budding and inclusion of high-density protein nanoclusters (Fig. 2c and 2d). Together, these data suggest the successful polarization of M1 macrophages from M0 macrophages.

3.2 The Isolation and characterization of M1-Exo

M1-Exo were isolated by differential centrifugation from incubation medium of M1 macrophages. M1-Exo exhibited a round and cup-like morphology with varying sizes (Fig. 3a and 3d). The M1-Exo were approximately 180 nm in size and exhibited a negative zeta potential (Fig. 3b and 3c). The concentration of M1-Exo was determined using a BCA assay after exosome collection (Fig. 3e). Next, we verified the presence of CD16 and SIRP-α on M1-Exo; CD63 was also identified on M1-Exo, consistent with its role in ESCRT recruitment during ILV formation (Fig. 3f). Because ILV formation involves inward budding of the cell membrane, the membrane-bound forms of CD16 and SIRP-α are incorporated into exosomes. Notably, PD-1 was also observed on M1-Exo (Fig. 3f). Together, these data demonstrate the successful isolation of M1-Exo with the desired immune checkpoint proteins and exosomal characteristics.

3.3 The initial biological attributes of M1-Exo

To observe the initial characteristics of M1-Exo in a tumor environment, B16F10 cells that express CD47 were used. We then incubated M1-Exo with B16F10 for 15 min, and intense binding of M1-Exo was initially observed (Fig. 4a). However, M1-Exo demonstrated minimal cytotoxicity as assessed by the Cell Counting Kit-8 (CCK-8) assay (Fig. 4b). Interestingly, caspase-3 was expressed in B16F10 cells after 24 h (Fig. 4c). Together, these data demonstrated the binding and biocompatibility of M1-Exo, while also indicating the necessity of combined chemotherapy delivery.

3.4 The doxorubicin loading and biological attributes of M1-Exo/DOX

To study doxorubicin loading into M1-Exo via electroporation and validate chemotherapy delivery, suitable loading voltage and doxorubicin concentration were determined by measuring autofluorescence at 560–595 nm upon blue light excitation (Fig. 5a and 5b). After 24 h of incubation, B16F10 cells treated

with M1-Exo/DOX showed significantly higher nuclear doxorubicin accumulation than those treated with free doxorubicin, due to exosome-mediated endocytosis and subsequent nuclear translocation (Fig. 5c). Furthermore, M1-Exo/DOX induced a significant increase in apoptosis of B16F10 cells, as analyzed by APC Annexin-V/PI flow cytometry, with the majority of cells in early-stage apoptosis (Fig. 5d). Together, these results reveal the successful construction and function of M1-Exo/DOX.

4. Discussion

The successful polarization of M1 macrophages from M0 macrophages using LPS was confirmed by morphological changes and upregulation of CD80/CD86. Super-resolution imaging further revealed nanoclusters of CD16 and SIRP-α on pseudopods, which are high-frequency sites of endocytosis, suggesting that these membrane proteins are incorporated into exosomes during their formation through inward budding. This observation supports the rationale for using M1 macrophages as a source of exosomes with inherited immune checkpoint proteins.

Building on these findings, the isolated M1-Exo exhibited typical exosome characteristics, including round/cup-like morphology, a size of approximately 180 nm, and a negative zeta potential, a negative zeta potential, which may favor tissue penetration and reduce hemolysis *in vivo*. Western blotting confirmed the presence of CD16, SIRP-α, and notably PD-1 on M1-Exo. The identification of PD-1 on M1-Exo raises the possibility of PD-1:PD-L1 axis immune checkpoint blockade. Li *et al*. (2022) demonstrated that engineered T cell extracellular vesicles displaying PD-1 boost anti-tumor immunity [17]. The cooperation of multiple ICIs could constitute a platform with greater specificity through binding affinity adjustments, involving both strong and weak ligands that eventually eliminate each respective non-specific binding for each ICI. Therefore, the PD-1 expressed on M1-Exo suggests initial opportunities for developing this multi-ICI platform.

Next, we examined the functional interaction of M1-Exo with cancer cells. The intense binding of M1-Exo to B16F10 cells within 15 min indicates efficient recognition of CD47. However, the minimal cytotoxicity of M1-Exo alone (Fig. 4b) suggests that the innate pro-apoptotic effect of M1-Exo is weak, justifying the need for doxorubicin loading. The observed expression of caspase-3 in B16F10 after 24 h incubation with M1-Exo may be attributed to potential death ligands identified in the proteomics of M1-Exo [18]. Classically, caspase-3 plays a role during the execution phase of apoptosis and necrosis, activated by either the intrinsic pathway (via caspase-9) or the extrinsic pathway (via caspase-8), and functions as the main executor of apoptotic body formation [19]. More recently, Nano et al. (2023) characterized caspase-3-induced apoptosis as a heterogeneous response, with no specific caspase-3 concentration threshold that guarantees apoptosis; cell state variability can thus lead to conditional survival or apoptosis [20]. This complexity may be reflected in the expression of caspase-3 in B16F10 cells, which could be induced by M1-Exo but may also pre-exist. Furthermore, caspase-3 has demonstrated partially tumor-beneficial characteristics, including angiogenesis, proliferation, and migration [21]. These findings further underscore the goal of this study: to induce robust tumor cell death by utilizing the innate properties of exosomes to achieve effective chemotherapy delivery.

To address this goal, we loaded doxorubicin into M1-Exo via electroporation, which successfully achieved loading without disrupting exosome integrity. The enhanced nuclear accumulation of doxorubicin delivered via M1-Exo, compared to free doxorubicin, suggests efficient endocytosis and intracellular trafficking. The significant increase in early-stage apoptosis (Annexin V-positive/PI-negative) induced by M1-Exo/DOX confirms the synergistic effect of immune checkpoint blockade and chemotherapy. *In vivo* investigations in tumor-bearing mice would further demonstrate the specificity of M1-Exo/DOX. However, due to the presence of CD47 on red blood cells and hematopoietic stem cells, the innate functioning of the SIRP-α:CD47 axis poses potential challenges for in vivo administration of M1-Exo/DOX [22, 23]. Nevertheless, this system can be further enhanced by implementing pH-responsive release mechanisms, overexpressing ICIs, or using ICIs with improved binding affinity [17, 24, 25].

5. Conclusions

Utilizing the inflammatory properties of LPS-polarized M1 macrophages, we revealed nanoclusters of ICI proteins on pseudopods, which are regions with intense endocytosis, thus leading to the inheritance of these properties onto derived exosomes. Then we specifically found SIRP-α, CD16, and additionally PD-1 on stable and biocompatible M1-Exo. These ICIs undergo specific binding to CD47 and PD-L1 immune checkpoints on cancer cells, leading to blockade. There was a significant amount of binding to melanoma cancer cells after a short incubation. Furthermore, we validated the possibility of loading doxorubicin and other hydrophilic chemotherapeutics into exosomes while maintaining their functions, and furthermore added induced apoptosis to the M1-Exo platform. This research validated the theoretical functions of immune cell-derived exosomes as a nuanced multifunctional platform for immune checkpoint inhibition and drug delivery.

Declarations

Author Contributions: Conceptualization, X.B. and Y.F.; methodology, X.B. and Y.F.; software, M.X.; validation, M.X.; formal analysis, M.X.; investigation, X.B. and Y.F.; resources, G.J.; data curation, M.X; writing-original draft preparation, X.B. and Y.F.; writing-review and editing, C.D. and G.J.; visualization, M.X.; supervision, C.D and G.J.; project administration, X.B. and Y.F.; funding acquisition, M.X. and C.D.. All authors have read and agreed to the published version of the manuscript.

Funding: This research was funded by the Natural Science Foundation of Zhejiang Province (ZCLQ24C1002); and the Natural Science Foundation of Ningbo (2022J203). Mingsheng Xu was supported by China Postdoctoral Science Foundation (2025M782966) and Jiangsu Funding Program Excellent Postdoctoral Talent (2025ZB803).

Institutional Review Board Statement: Not applicable.

Conflicts of Interest: The authors declare no conflicts of interest.

Data availability: All data supporting the findings of this study are available within the paper and its Supplementary Information. Full-length blots are provided in Supplementary Figure S1 and S2.

References

1. Wang, Y. et al. Macrophage-derived extracellular vesicles: diverse mediators of pathology and therapeutics in multiple diseases. *Cell. Death Dis.* **11**, 924 (2020).
2. Tenchov, R., Bird, R., Curtze, A. E. & Zhou, Q. Exosomes—nature's lipid nanoparticles, a rising star in drug delivery and diagnostics. *ACS Nano*. **16,** 17802–17846 (2022).
3. Lau, N. C. H. & Yam, J. W. P. From exosome biogenesis to absorption: key takeaways for cancer research. *Cancers* **15**, 1992 (2023).
4. Escola, J. M. et al. Selective enrichment of tetraspan proteins on the internal vesicles of multivesicular endosomes and on exosomes secreted by human B-lymphocytes. *J. Biol. Chem.* **273** (32), 20121–20127 (1998).
5. Pardoll, D. M. The blockade of immune checkpoints in cancer immunotherapy. *Nat. Rev. Cancer*. **12**, 252–264 (2012).
6. Postow, M. A., Sidlow, R. & Hellmann, M. D. Immune-related adverse events associated with immune checkpoint blockade. *N Engl. J. Med.* **378**, 158–168 (2018).
7. Swain, A., Jena, S. R. & Samanta, L. Smart nanocarriers for cancer: harnessing exosomes and lipid systems in photodynamic and immunotherapy. *Front. Immunol.* **16**, 1687953 (2025).
8. Sreejit, G., Fleetwood, A. J., Murphy, A. J. & Nagareddy, P. R. Origins and diversity of macrophages in health and disease. *Clin. Transl Immunol.* **9**, e1222 (2020).
9. Schulz, C. et al. A lineage of myeloid cells independent of Myb and hematopoietic stem cells. *Science* **336**, 86–90 (2012).
10. Yan, L. et al. Macrophage plasticity: signaling pathways, tissue repair, and regeneration, MedComm 5 e658. (2024).
11. Sica, A. & Mantovani, A. Macrophage plasticity and polarization: in vivo veritas. *J. Clin. Invest.* **122**, 787–795 (2012).
12. Gundra, U. M. et al. Alternatively activated macrophages derived from monocytes and tissue macrophages are phenotypically and functionally distinct. *Blood* **123**, e110–e122 (2014).
13. Brancewicz, J., Wójcik, N., Sarnowska, Z., Robak, J. & Król, M. The multifaceted role of macrophages in biology and diseases. *Int. J. Mol. Sci.* **26,** 2107 (2025).
14. Koh, E. et al. Exosome-SIRPα, a CD47 blockade increases cancer cell phagocytosis. *Biomaterials* **121**, 121–129 (2017).
15. Wang, P. et al. Exosomes from M1-Polarized Macrophages Enhance Paclitaxel Antitumor Activity by Activating Macrophages-Mediated Inflammation. *Theranostics* **9** (6), 1714–1727 (2019).
16. Behrens, L. M., van den Berg, T. K. & van Egmond, M. Targeting the CD47-SIRPα innate immune checkpoint to potentiate antibody therapy in cancer by neutrophils. *Cancers* **14**, 3366 (2022).

17. Li, B. et al. Engineered T cell extracellular vesicles displaying PD-1 boost anti-tumor immunity. *Nano Today*. **46**, 101606 (2022).
18. Pantazi, P. et al. Quantitative proteomics reveals differential extracellular vesicle cargo from M1 and M2 monocyte-derived human macrophages. *Preprint bioRxiv* ; (2024). 2024.09.17.613483. Published 2024 Sep 21.
19. Porter, A. G. & Jänicke, R. U. Emerging roles of caspase-3 in apoptosis. *Cell Death Differ.* **6** (2), 99–104 (1999).
20. Nano, M., Mondo, J. A., Harwood, J., Balasanyan, V. & Montell, D. J. Cell survival following direct executioner-caspase activation. Proceedings of the National Academy of Sciences. ;120(4):e2216531120. (2023).
21. Feng, X., Wang, Y. W., He, S. J. & Huang, Q. The paradigm-shifting roles of caspase-3 in cancer: from death towards resuscitation. *Cancer Cell Int.* **26** (1), 93 (2026).
22. Jaiswal, S. et al. CD47 is upregulated on circulating hematopoietic stem cells and leukemia cells to avoid phagocytosis. *Cell* **138**, 271–285 (2009).
23. Oldenborg, P. A. et al. Role of CD47 as a marker of self on red blood cells. *Science* **288** (5473), 2051–2054 (2000).
24. Guo, Y. et al. pH-activated nanoplatform derived from M1 macrophages' exosomes for photodynamic and ferroptosis synergistic therapy to augment cancer immunotherapy. *Biomat Res.* **29**, 0153 (2025).
25. Weiskopf, K. et al. Engineered SIRPα variants as immunotherapeutic adjuvants to anticancer antibodies. *Science* **341**, 88–91 (2013).
26. Leblanc, P. et al. Isolation of exosomes and microvesicles from cell culture systems to study prion transmission. *Methods Mol. Biol.* **1545**, 153–176 (2017).
27. Szatanek, R., Baran, J., Siedlar, M. & Baj-Krzyworzeka, M. Isolation of extracellular vesicles: determining the correct approach (Review). *Int. J. Mol. Med.* **36**, 11–17 (2015).

Figures

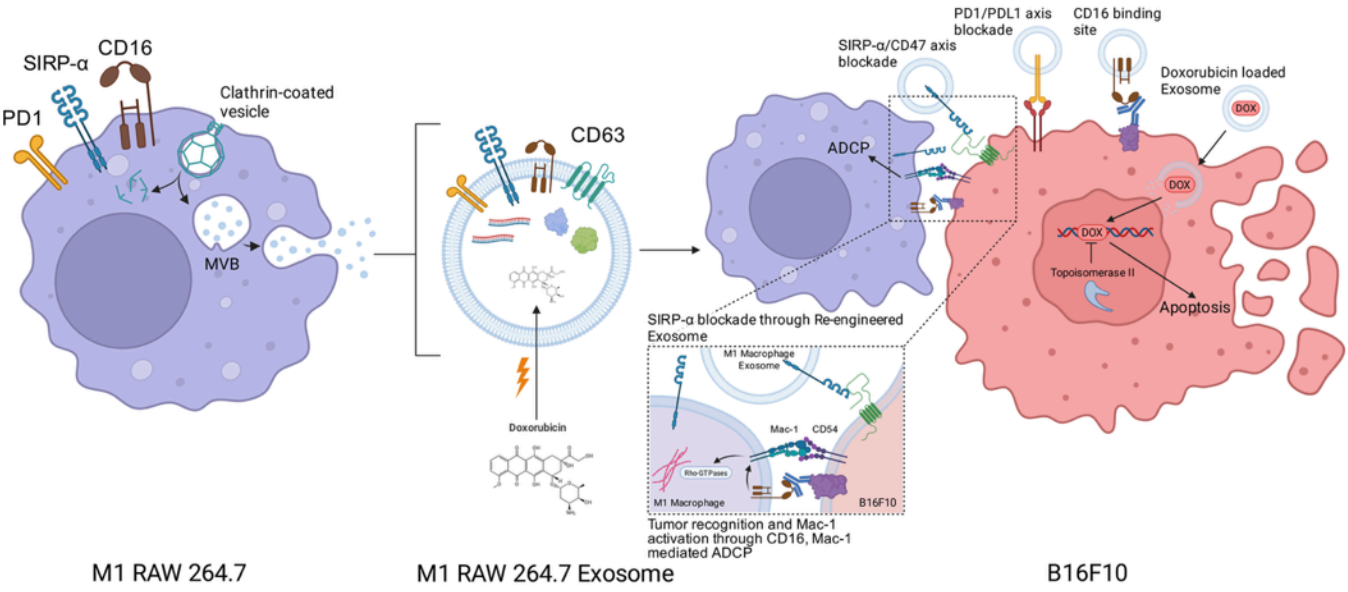


Figure 1

Schematic illustration of the formation of M1-Exo from M1 Raw 264.7 cells, electroporation-mediated drug loading of M1-Exo, and the interaction of M1-Exo/DOX with B16F10 cells.

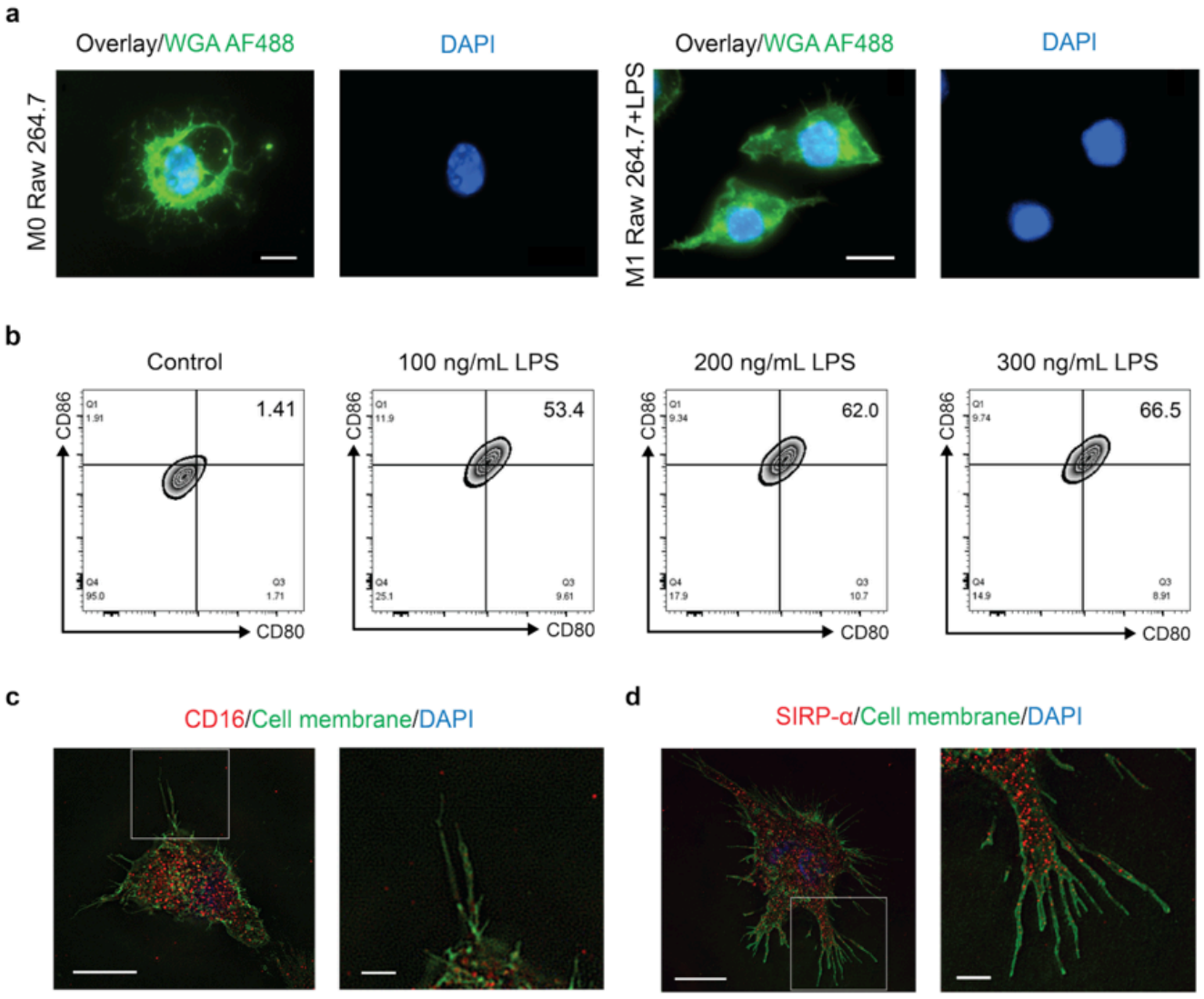


Figure 2

Characterization of polarized M1 macrophages. (a) Morphology of M0 Raw 264.7 cells (left) and M1 Raw 264.7 cells (right). Scale bar: 10 μm. (b) Flow cytometry analysis of M1 polarization markers CD80 and CD86 at different LPS concentrations (control, 100 ng/mL, 200 ng/mL, 300 ng/mL). (c, d) Super-resolution images (scale bar: 10 μm) and close-up views of pseudopods (scale bar: (c) 5 μm, (d) 2.5 μm) of (c) CD16 on M1 Raw 264.7 cells and (d) SIRP-α on M1 Raw 264.7 cells.

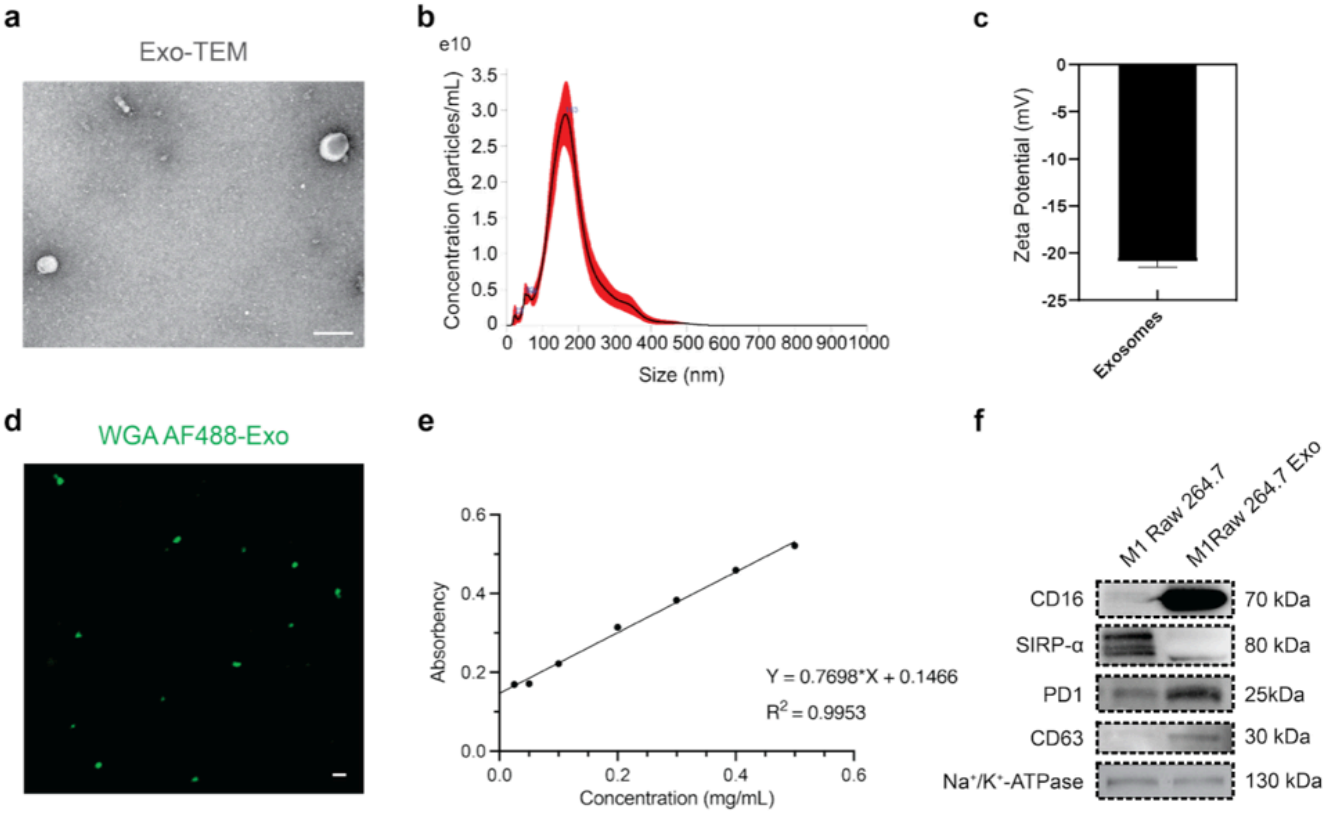


Figure 3

Characterization of M1 Raw 264.7-derived exosomes. (a) TEM image of M1-Exo. Scale bar: 200 nm. (b) Size distribution of M1-Exo analyzed by nanoparticle tracking analysis (180.1 ± 7.3 nm). (c) Zeta potential of M1-Exo analyzed by electrophoretic light scattering. (d) Confocal image of M1-Exo. Scale bar: 1 μm. (e) Standard curve for M1-Exo concentration determined by BCA assay. (f) Western blot analysis of CD16, SIRP-α, PD-1, and the surface marker CD63 in M1 Raw 264.7 cells and M1-Exo.Western blot analysis of CD16, SIRP-α, PD-1, and the surface marker CD63 in M1 Raw 264.7 cells and M1-Exo. Blots were obtained from different gels (indicated by dashed borders). Full-length blots are provided in Supplementary Fig. S1.

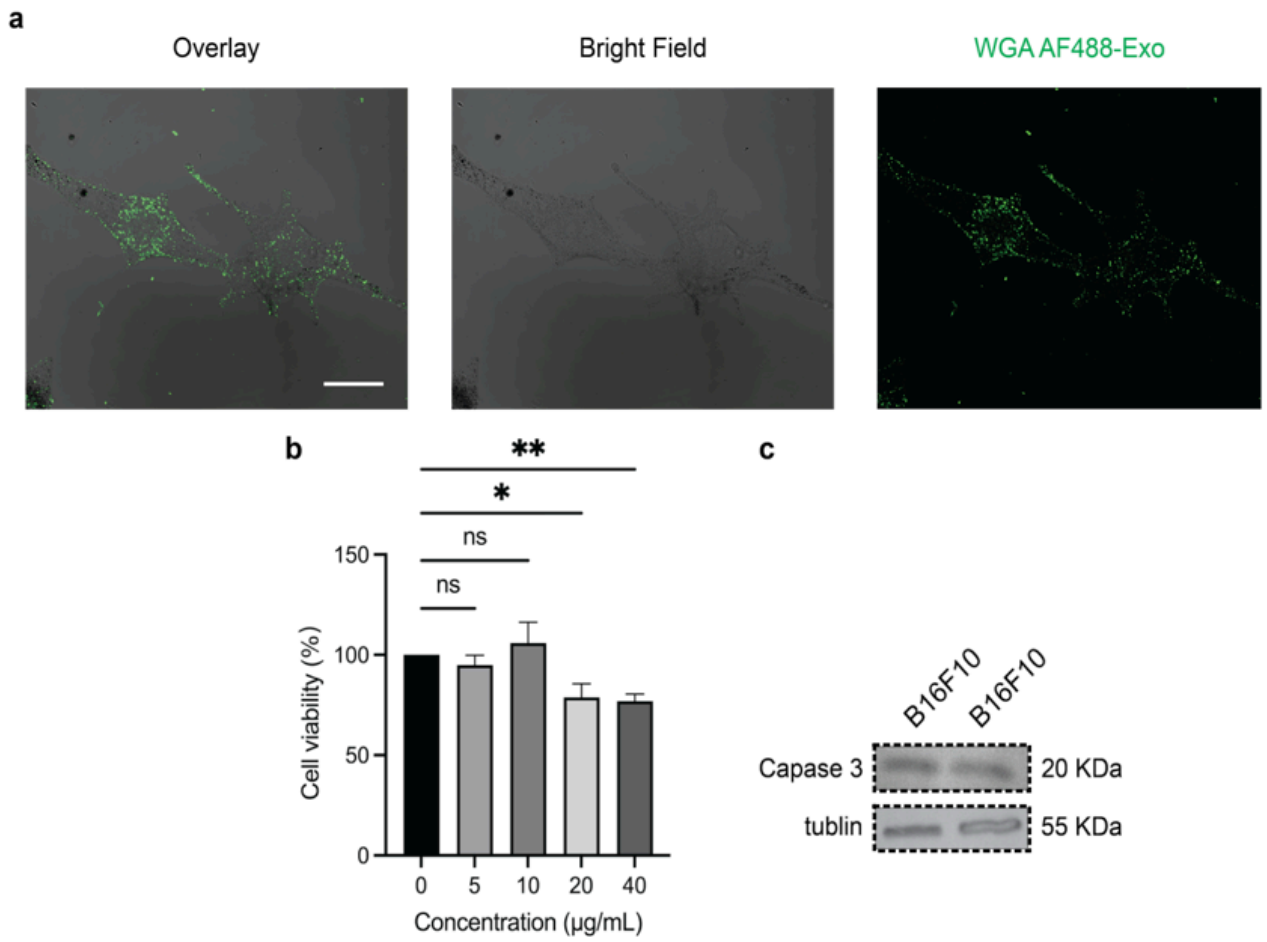


Figure 4

Biological attributes of M1-Exo. (a) Confocal images of B16F10 cells incubated with M1-Exo for 15 min *in vitro*. Scale bar: 20 μm. (b) Cell viability of B16F10 cells incubated with the indicated concentrations of M1-Exo for 24 h *in vitro* (n = 9). PBS-treated cells served as the control group. Data are shown as mean ± SEM. (c) Western blot analysis of caspase-3 in B16F10 cells incubated with M1-Exo (100 μg/mL) for 24 h *in vitro*. Blots were obtained from different gels (indicated by dashed borders). Full-length blots are provided in Supplementary Fig. S2.

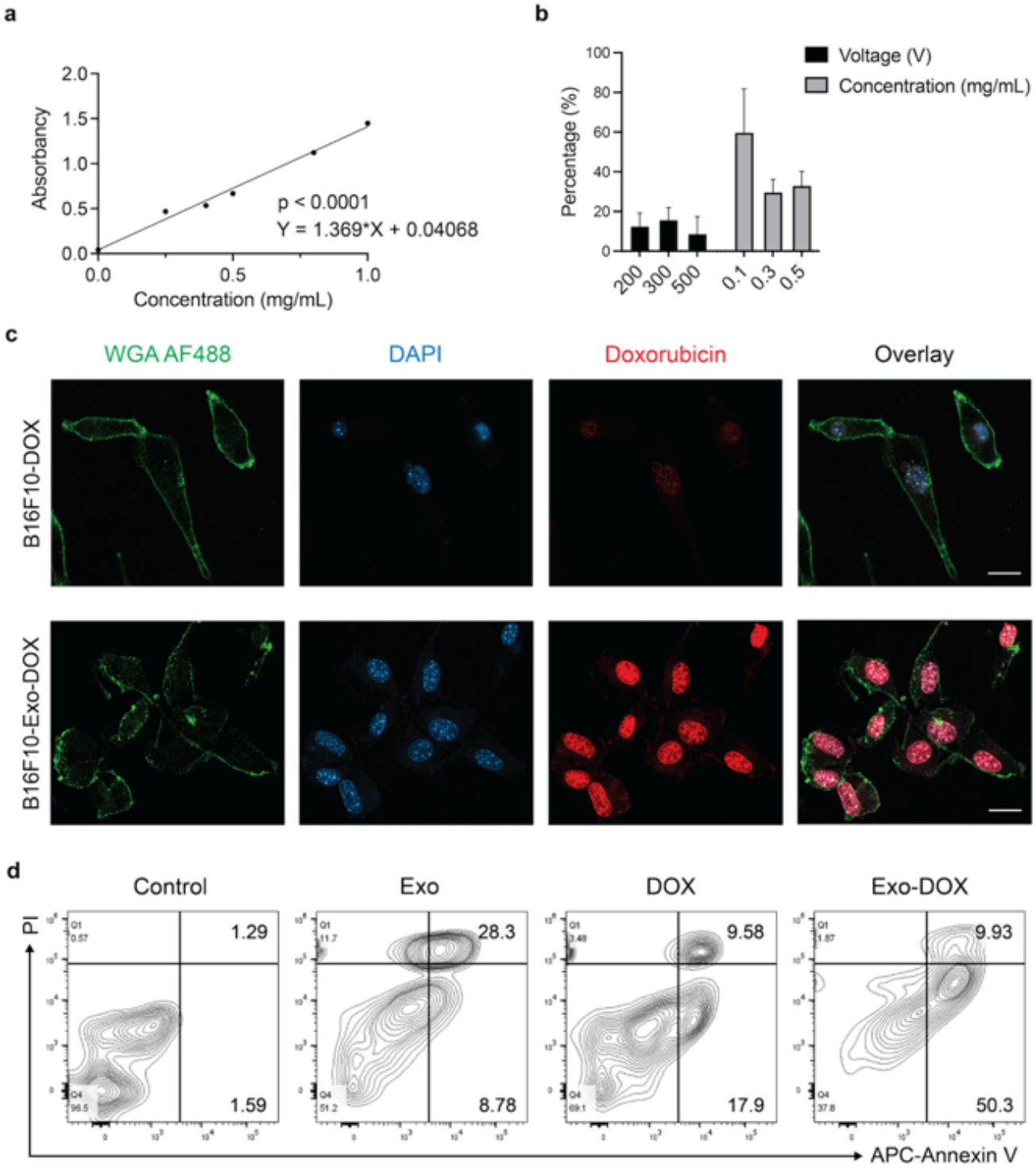


Figure 5

Biological attributes of M1-Exo/DOX. (a) Standard curve for DOX loading efficiency via DOX autofluorescence. (b) Percentage loading efficiency of M1-Exo/DOX under different loading conditions as indicated (n = 3). (c) Confocal images of B16F10 cells after 3 h *in vitro* incubation with DOX and M1-Exo/DOX. Scale bar: 20 μm. (d) Representative Annexin V/PI flow cytometry plots of B16F10 cells after 24 h incubation with PBS (control), 100 μg/mL M1-Exo, 25.5 μg/mL DOX, or M1-Exo/DOX.

Supplementary Files

This is a list of supplementary files associated with this preprint. Click to download.

- SupplementaryFig.S2.docx
- SupplementaryFig.S1.docx